

High-speed focus-induced photoresponse in amorphous silicon photodetectors for optical distance measurements

Andreas Bablich, Maurice Müller, Paul Kienitz, Rainer Bornemann, and Peter Haring Bolívar

Department of Electrical Engineering and Computer Science, School of Science and Technology, Centre for Sensor Systems, University of Siegen, Germany

Email: andreas.bablich@uni-siegen.de

The Focus-Induced Photoresponse (FIP) enables 3D sensing capabilities by evaluating the irradiance dependent non-linear detector response in defect-based materials. Since this advantage is intricately associated to a slow response, the electrical bandwidth of previous FIP sensors is limited to a few kHz only. We report the FIP in amorphous silicon pin photodiodes and propose a sensor read out based on a harmonics analyses. We achieve modulation frequencies of 500 kHz and a non-linear beat frequency detection up to at least 3.5 MHz, surpassing the bandwidth of state-of-the-art architectures by at least a factor of 175. The FIP sensors further achieve signal-to-noise ratios of ~50 dB, depth resolutions of at least 5.4 mm at 126 cm and a DC FIP detection limit of $1.3 \mu\text{W}/\text{mm}^2$.

Introduction: As applications advance, fast, precise, low-noise and high-resolution 3D-scene detection is a key technology enabler for a wide range of applications such as autonomous driving, autonomous systems, non-invasive diagnosis and surgery, and for future manufacturing. Reliable state-of-the-art 3D imagers utilize the ToF principle, relying on laser technology and sophisticated sensors. Imager fill-factors stagnate at ~22% for conventional photonic mixer devices (PMD) [1] or ~13% for novel gated single-photon avalanche diodes (SPAD) [2], respectively. However, megapixel SPAD cameras can achieve depth resolutions of 7.8 mm and enable 2D/3D scene detection up to 2 m [2]. Conventional PMD based 3D imagers detect distances up to ~6 m and achieve a depth resolution of ~7 cm at 1 m [3]. Although alternative light detection and ranging (LIDAR) sensors enable distance measurements exceeding 10 m, this concept has significant drawbacks with respect to achievable depth resolutions and most importantly on scalability, even in miniaturized designs [4]. The focused-induced photoresponse (FIP) is a novel, ultra-sensitive 3D-imaging technique in defective materials based on irradiance dependent responsivity changes [5] waiving subsequent data processing for image reconstruction. Simultaneous sensor read-out at different foci enables:

- (I) maximum scalability (depth information can directly be extracted from the incident light from a single viewpoint) and fill-factors of 100 % [6, 7],
- (II) highly precise distance measurements with depth resolutions in the μm -range [5], and
- (III) low-light-level detection ($\mu\text{W}/\text{mm}^2$).

Although state-of-the-art FIP sensors combine several highly attractive advantages, comparatively low cut-off frequencies stagnate at very low bandwidths, severely restricting their widespread application. This restriction stems from photodetector technologies based on high defect densities and low charge carrier mobility materials, preventing a fast optical distance acquisition above 20 kHz [5, 8, 9]. Here, we present FIP detector technologies based on amorphous silicon that resolve such bandwidth limitations and expand photodetector speed by more than two orders of magnitude utilizing just one single-pixel photodetector.

Devices and methodology:

A. Device fabrication: Amorphous silicon (a-Si:H) pin photodetectors ($A = 2.88 \text{ mm}^2$) are grown on glass substrates by plasma-enhanced chemical vapour deposition (PECVD) in a MVS multi-chamber vacuum system at substrate temperatures below 200°C. Electrical contacts

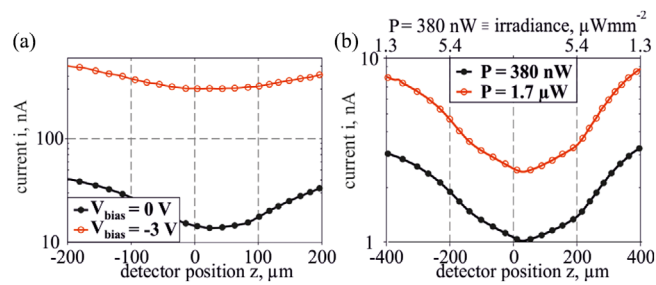


Fig. 1 (a) Bias-, (b) irradiance dependent z-Scan characteristics of the a-Si:H focused-induced photoresponse (FIP) detector

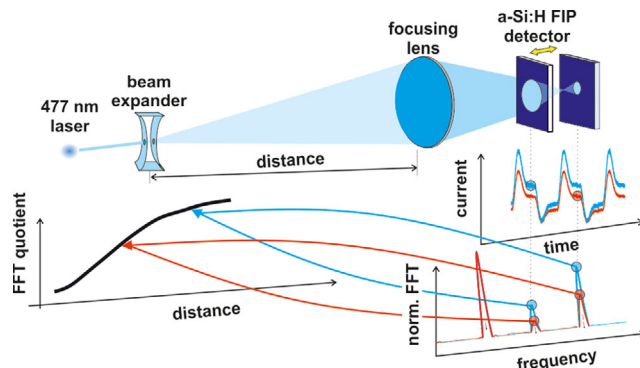


Fig. 2 Distance measurement setup exploiting the frequency-dependent focused-induced photoresponse (FIP) in a-Si:H sensors

consist of a transparent conductive oxide and are deposited in a radio-frequency sputtering tool at room temperature. Subsequently, the devices are structured by contact UV-lithography, packaged and contacted via wedge bonding.

B. Device characterization and simulation: Confocal microscopy at 488 nm has been used to determine bias and power-dependent z-Scan characteristics. Measurements utilize the optical setup shown in Figure 2 including a 477 nm laser module. The optical power on the sensor of 7.6 mW corresponds to an irradiance of $\sim 2 \times 10^{18} \text{ cm}^{-2} \text{ s}^{-1}$ if the detector is placed in focus. Subsequent $I-V$ conversion of the sensor output is necessary for transient and FFT data acquisition (2.5 GS/s). FFT signal quotients (Figure 6a) are recorded utilizing a 477 nm laser module with an optical power on the sensor of 4.1 mW. Focused ion-beam cross-sectioning, environmental scanning electron microscopy (Figure 6b), and stylus profilometry have been used to determine layer thicknesses, deposition homogeneity and reproducibility.

Results and discussion: The z-scan technique is used to precisely determine and quantify the irradiance dependent non-linear a-Si:H detector response by moving a focused laser cone vertically along the structure. Z-scan measurements have been conducted to quantify the FIP in a Si:H photodiodes enabling high-sensitive optical distance measurements [5]. At 488 nm, a non-linear current breakdown occurs at 380 nW corresponding to irradiances down to at least $1.3 \mu\text{W}/\text{mm}^2$ far out of focus as seen in Figure 1b. Those irradiances can easily be achieved utilizing low-cost light sources, for example, flashlights or LEDs renouncing expensive laser technology. For optical distance measurements, we find the ideal device-specific bias voltage V_{bias} to be 0 V (Figure 1a).

Subsequently, distance measurements based on the non-linear FIP have been performed utilizing the setup shown in Figure 2 with a modulation frequency f_{mod} of 500 kHz and 0 V bias voltage. In the proposed model, we re-construct reflected light from a diffuse reflecting object at a specific distance utilizing a light source, a beam expander and a focusing lens enabling the FIP as proposed in [5].

The detector transients reveal overshoots at the rising and falling edges (Figure 3a, yellow marks) due to slow defect filling [10]. We conclude and further exploit that the trap filling mechanism itself is changing significantly with the measured distance.

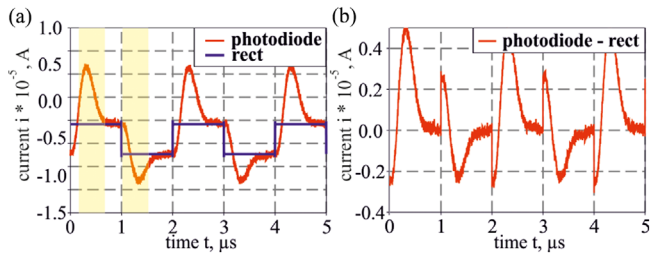


Fig. 3 (a) Time-domain and idealized rectangular detector signal, (b) time-domain sensor signal subtracted by the ideal rectangular sensor response

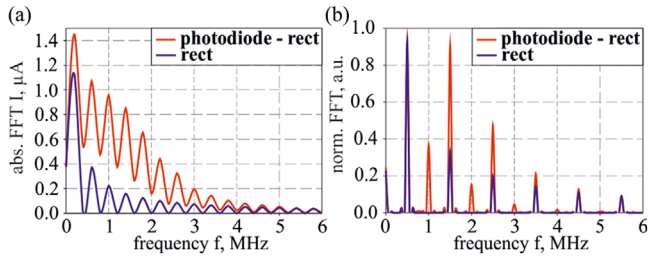


Fig. 4 (a) FFT of the rectangular and the subtracted signal response as shown in Figure 3b, (b) norm. FFT spectra of the signals shown in (a) verifying that non-linear beat frequency generation results from the time-domain diode signal

In the frequency domain, additional beat frequencies arise in the FFT spectrum originating from the defect-related overshoot that initially has been separated from the idealized sensor output (Figure 3b; Figure 4). Absolute FFT spectra for $d = 110$ cm and $d = 142$ cm are shown in Figure 5a. Besides the expected harmonics at frequency positions $(2 \cdot n + 1) \cdot f_{\text{mod}}$, additional beat frequencies occur at $(2 \cdot n) \cdot f_{\text{mod}}$. Measuring peak amplitudes at two different frequency positions

$$n \cdot f_{\text{mod}} \wedge m \cdot f_{\text{mod}}; n \neq m; n, m \neq 0 \quad (1)$$

and normalizing the FFT spectra to the peak amplitude of f_{mod} (Figure 5b,c) allows for a fast and unambiguous distance determination and distinction.

In this work, the non-linear current breakdown can clearly be verified up to an electrical bandwidth of at least 3.5 MHz (Figure 5c) that is 175 times higher than the best reported value in [9]. Since the achievable bandwidth depends on a variety of parameters, for example, the detector area, the light-absorbing material composition and thickness, defect densities, contact resistances, the device architecture itself and so forth, we expect significant improvements in the future with bandwidth optimized designs. Increasing f_{mod} further boosts the signal-to-noise ratio (SNR) as the $1/f$ noise in a-Si:H photodiodes is reduced significantly [11]. The SNR obtains a high dynamic of ~ 50 dB (Figure 5d) so that irradiances can further be reduced in future experiments. Besides boosting modula-

Table 1. a-Si:H FIP sensor performance and benchmarks: illumination wavelength, cut-off frequency, bias tunability, and number of pixels required for optical distance measurements

Material/device	TiO ₂ /DSSC	PbS/photo-conductor	TiO ₂ /DSSC	BDP-OMe:C60/OPD	a-Si:H/pin-diode
λ (nm)	530	1.550	730/850	850	477
f_{max} (kHz)	0.965	0.606	1	20	3.500
$f_{\text{mod,max}}$ (kHz)	0.965	0.606	1	20	500
Bias tunable	No	No	No	No	Yes
Irradiance (μ W/mm ²)	10	0.3	N/A	2	1.3
Sensor count	2	2	2	2	1
Encapsulation	Yes	Yes	Yes	Yes	No
Q' @ a specific distance	± 0.1 % @ 52 cm	N/A	N/A	N/A	± 0.43 % @ 1.26 m
Depth resolution Δd	500 μ m				5.4 mm
Ref.	[5]	[5]	[8]	[9]	This work

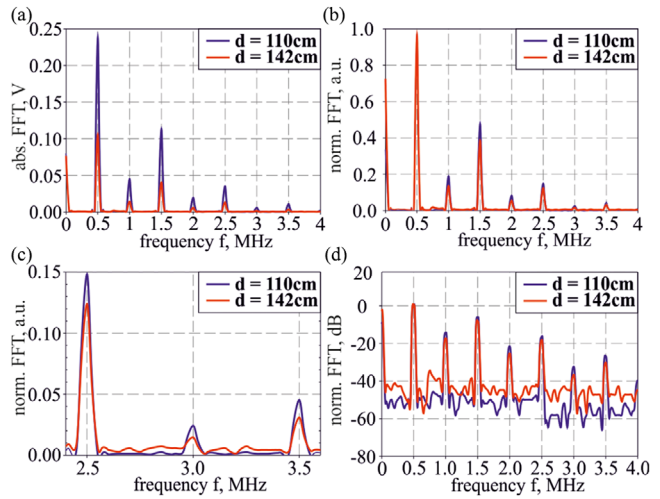


Fig. 5 Distance measurement results: (a) Absolute FFT spectra, (b) FFT spectra normalized on the signal amplitude at f_{mod} , (c) normalized FFT shown for a bandwidth of 2.4–3.6 MHz, (d) signal-to-noise ratio (SNR) extracted from (b). All results are shown for $d = 110$ cm and $d = 142$ cm, 500 kHz modulation and 477 nm illumination

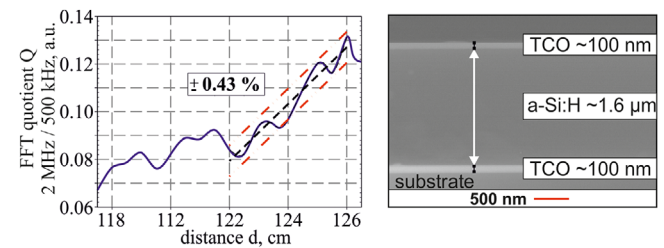


Fig. 6 (left) Distance dependent FFT signal measured at 2 MHz and normalized to the FFT response at $f_{\text{mod}} = 500$ kHz for 444 nm, (right) cross-sectional ESEM of an a-Si:H FIP photodetector

tion frequencies, optimized device designs can enable significant SNR improvements in the future, for example, by applying a proper electrical field engineering across the absorber, to further increase FIP detector responsivities.

We further define an FFT signal quotient Q of two current amplitudes $I_{1,2}$ at two different measurement frequencies $f_{1,2}$ to determine the distance d , to estimate the depth resolution Δd and to eliminate influences of the total light power as shown in Equation (3)

$$Q = I_2(f_2) / I_1(f_1) \quad (3)$$

In Figure 6a, we exemplarily show Q normalized on $f_1 = f_{\text{mod}} = 500$ kHz for the 2nd beat frequency located at $f_2 = 2$ MHz. The maximum relative deviation Q' of Q represents the

achievable depth resolution at a specific distance. Fitting Q with linear regression results in $Q' = \pm 0.43\%$ at $d = 1.26$ m and a corresponding depth resolution of $\Delta d = 5.4$ mm.

On-chip, the proposed sensor readout can easily be integrated, for example, by integrating two narrow bandpass filters for signal acquisition at two fixed measurement frequencies in combination with a current or voltage divider circuit to calculate signal quotients enabling unambiguous distance determination. Achieving $\pm 0.43\%$ precision is comparable to values previously reported in [5]. A brief performance comparison of a-Si:H based FIP detectors with state-of-the-art devices is given in Table 1.

Conclusion: We systematically investigated the irradiance dependent current breakdown in a-Si:H pin photodetectors and experimentally demonstrate single-pixel distance measurements at read-out frequencies up to at least 3.5 MHz and 500 kHz modulation, more than two orders of magnitude higher than previous FIP device demonstrations. Achieving a SNR of ~ 50 dB and depth resolutions of at least 5.4 mm at a distance of 1.26 m are very promising results for high-dynamic, high-resolution and high-speed 3D imaging. Low-temperature PECVD fabrication enables back-end integration on top of silicon electronics with fill factors of 100% and allows tailoring sensor architecture and properties for application-specific purposes.

Acknowledgements: The authors gratefully acknowledge the German Description Fund for Regional Development (EFRE0200545) for funding this research project. We also thank the Micro- and Nanoanalytics Facility (MNaF) and the Institute of Chemistry for Building Materials of the University of Siegen for FIB-cross sectioning and ESEM sample analyses

Conflict of interest: We declare that we do not have any commercial or associative interest that represents a conflict of interest in connection with the work submitted.

Data availability statement: Data available on request from the authors

© 2022 The Authors. *Electronics Letters* published by John Wiley & Sons Ltd on behalf of The Institution of Engineering and Technology

This is an open access article under the terms of the Creative Commons Attribution-NonCommercial-NoDerivs License, which permits use and distribution in any medium, provided the original work is properly cited, the use is non-commercial and no modifications or adaptations are made.

Received: 27 November 2021 Accepted: 9 February 2022

doi: 10.1049/ell2.12450

References

- 1 Lange, R., Böhmer, S., Buxbaum, B.: 11 - CMOS-based optical time-of-flight 3D imaging and ranging. In: D. Durini (ed.), *High Performance Silicon Imaging*, 2nd ed, pp. 319–375. Sawston, Cambridge: Woodhead Publishing, (2020). <https://doi.org/10.1016/B978-0-08-102434-8.00011-8>
- 2 Morimoto K., Ardelean A., Wu M.-L., Ulku A. C., Antolovic I. M., Bruschini C., Charbon E.: Megapixel time-gated SPAD image sensor for 2D and 3D imaging applications. *Optica*. **7**(4), 346 (2020). <https://doi.org/10.1364/optica.386574>
- 3 Condotta, I.C.F.S., Brown-Brandl, T.M., Pitla, S.K., Stinn, J.P., Silva-Miranda, K.O.: Evaluation of low-cost depth cameras for agricultural applications. *Comput. Electron. Agric.* **173**, 105394 (2020) <https://doi.org/10.1016/j.compag.2020.105394>.
- 4 Royo S., Ballesta-Garcia M.: An Overview of Lidar Imaging Systems for Autonomous Vehicles. *Appl. Sci.* **9**(19), 4093 (2019). <https://doi.org/10.3390/app9194093>
- 5 Pekkola, O. et al.: Focus-Induced Photoresponse: a novel way to measure distances with photodetectors. *Sci. Rep.* **8**(1), 9208 (2018) <https://doi.org/10.1038/s41598-018-27475-1>.
- 6 Lule, T. et al.: Sensitivity of CMOS based imagers and scaling perspectives. *IEEE Trans. Electron Devices* **47**(11), 2110–2122 (2000) <https://doi.org/10.1109/16.877173>.
- 7 Lemmi, F., Rahn, J.T., Street, R.A.: Lateral conduction in structured amorphous silicon p+-i-n+ photodiodes. *J. Non Cryst. Solids* **266–269**, 1203–1207 (2000) [https://doi.org/10.1016/S0022-3093\(99\)00925-4](https://doi.org/10.1016/S0022-3093(99)00925-4).
- 8 Kasparavicius, E. et al.: Focus-induced photoresponse technique-based NIR photodetectors containing dimeric polymethine dyes. *J. Electron. Mater.* **48**(9), 5843–5849 (2019) <https://doi.org/10.1007/s11664-019-07375-4>.
- 9 Wang, Y., Benduhn, J., Baisinger, L., Lungenschmied, C., Leo, K., Spoltore, D.: Optical distance measurement based on induced non-linear photoresponse of high-performance organic near-infrared photodetectors. *ACS Appl. Mater. Interfaces* **13**(19), 23239–23246 (2021) <https://doi.org/10.1021/acsami.1c04705>.
- 10 Ulrichs, C., Eickhoff, Th., Wagner, H.: Transient response of the photocurrent in a-Si:H layers and solar cells. *J. Non Cryst. Solids* **164–166**, 705–708 (1993) [https://doi.org/10.1016/0022-3093\(93\)91095-K](https://doi.org/10.1016/0022-3093(93)91095-K).
- 11 Blecher, F., Schneider, B., Sterzel, J., Böhm, M.: Noise of a-Si:H Pin diode pixels in imagers at different operating conditions. *MRS Online Proc. Lib.* **557**, 869–874 (1999) <https://doi.org/10.1557/PROC-557-869>.